A study of stratospheric GW fluctuations and sporadic E at midlatitudes with focus on possible orographic effect of Andes

Klemens Hocke and Toshitaka Tsuda
Radio Science Center for Space and Atmosphere, Kyoto University, Uji, Kyoto, Japan

Alejandro de la Torre
Departamento de Fisica, Facultad de Ciencias Exactas y Naturales, Universidad de Buenos Aires, Buenos Aires, Argentina

Received 24 September 2001; revised 11 January 2002; accepted 20 March 2002; published 23 October 2002.

[1] Longitudinal dependences of stratospheric gravity wave (GW) fluctuations and lower ionospheric irregularities (sporadic E) at midlatitudes are studied by means of radio occultation data of the Global Positioning System/Meteorology Experiment (GPS/MET) satellite mission. The zonal average of temperature variance of GW fluctuations with vertical scales less than 7 km at northern midlatitudes is observed to be similar to that at southern midlatitudes, but there is a significant interhemispheric difference in the longitudinal dependence of GW fluctuations. The GPS/MET data at northern midlatitudes show a rapid change of the gravity wave distribution from 25 to 35 km height, resulting in a broad maximum of temperature variance located over the Atlantic and Eurasia. We only find in the wave distribution at $h = 25$ km some weak traces of possible orographic effects. On the other hand, the distribution of GW fluctuations at southern midlatitudes has a strong and sharp maximum over Andes, which is obviously due to orographic wave generation by the interaction of surface wind with the Andean mountain ridge. This observation of the new GPS radio occultation technique is in agreement with previous measurements of spaceborne microwave and infrared limb sounders. The amplitude of the average wave field increases with height over Andes, while the amplitude maximum moves westward, against the prevailing wind. The temperature fluctuations have an apparent, dominant vertical wavelength of around 6 km. In situ measurements by a balloon-borne rawinsonde at Ushuaia, Argentina (54.7°S, 68.1°W) are compared to a simultaneous GPS/MET temperature profile. The balloon observations of temperature and horizontal wind are interpreted by a large amplitude mountain wave propagating to the upper stratosphere. Wave characteristics and atmospheric background conditions are investigated in detail for this mountain wave observation. Finally, the GPS/MET experiment indicates enhanced sporadic E in the lower ionosphere over Southern Andes. We assume that these plasma irregularities are generated by enhanced, upward wave flux due to the possible orographic effect of Andes. *INDEX TERMS:* 3362 Meteorology and Atmospheric Dynamics: Stratosphere/troposphere interactions; 3384 Meteorology and Atmospheric Dynamics: Waves and tides; 3322 Meteorology and Atmospheric Dynamics: Land/atmosphere interactions; 2427 Ionosphere: Ionosphere/atmsophere interactions (0335); 2439 Ionosphere: Ionospheric irregularities; *KEYWORDS:* stratospheric gravity waves, sporadic E, GPS radio occultation, orographic waves, mountain wave propagation, Andes

Citation: Hocke, K., T. Tsuda, and A. de la Torre, A study of stratospheric GW fluctuations and sporadic E at midlatitudes with focus on possible orographic effect of Andes, *J. Geophys Res.*, *107*(D20), 4428, doi:10.1029/2001JD001330, 2002.

1. Introduction

[2] Temperature fluctuations of high resolution profiles are analyzed and discussed for investigation of global and regional distributions of stratospheric gravity waves (GWs) at midlatitudes. To begin with we survey some previous observational and theoretical works on stratospheric gravity waves and their origin.

Copyright 2002 by the American Geophysical Union.
0148-0227/02/2001JD001330

[3] At midlatitudes, lower atmospheric wind can generate gravity waves by orographic effect [*Nastrom and Fritts*, 1992]. The Earth's topography also has influence on locations of jet streams of eastward geostrophic wind at midlatitudes. The jet streams are variable due to seasonal geostrophic wind adjustments and achieve their maximal wind speeds over oceanic areas. Variability and shear flow of jet streams are important sources of gravity waves at midlatitudes [*Fritts and Nastrom*, 1992; *Murayama et al.*, 1994]. Convective clouds in the lower troposphere can be

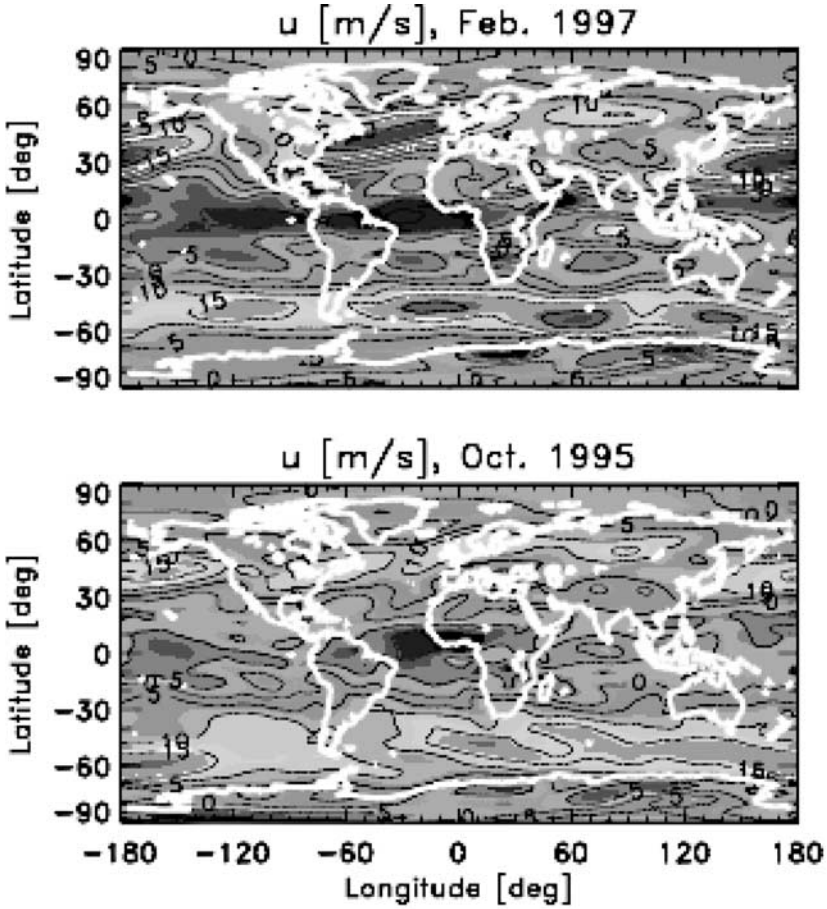

Figure 1. Global map of zonal wind at pressure level 700 mbar in February 1997 (top) and October 1995 (bottom). Red (blue) color denotes eastward (westward) wind direction respectively. Contour labels are in [m/s]. The zonal wind data were calculated and provided by NCEP/NCAR reanalysis and Climate Diagnostics Center (CIRES/NOAA). See color version of this figure at back of this issue.

regarded as dominant gravity wave source at low latitudes in the tropics [*McLandress et al.*, 2000; *Vincent and Alexander*, 2000]. To some extent convectively generated gravity waves are also present in the subtropics and at midlatitudes [*Fritts and Nastrom*, 1992; *Preusse et al.*, 2001]. Gravity wave generation is in addition observed during meteorological disturbances such as fronts, thunderstorms, or typhoons [*Sato*, 1993].

[4] Gravity waves propagating from tropospheric source regions up to the stratosphere may experience a manifold of interactions on their way. Due to the exponential decrease of air density with height and conservation of wave action, gravity wave amplitudes are increasing. This increase can lead to breaking or dissipation of gravity waves in the stratosphere, forcing together with planetary waves the mean circulation of the stratosphere. Further dynamic processes are wave-wave interaction, wave ducting by background wind, wave generation by shear flow, and wave absorption by critical wind levels. All these processes have influence on the distribution of gravity waves while propagating from the troposphere to the stratosphere [*Fetzer and Gille*, 1994; *Alexander and Vincent*, 2000]. The relationship between tropospheric gravity wave sources and stratospheric wave activity is only obvious for isolated and strong tropospheric gravity wave sources such as convection zones in the tropics and orographic waves from Andes [*McLandress et al.*, 2000; *Hocke and Tsuda*, 2001; *Preusse et al.*, 2001].

[5] *Alexander* [1998] explains that many puzzles and misinterpretations of atmospheric data are due to limits of observation techniques, e.g., limited measurement ranges of atmospheric wavelengths and frequencies. Continuous sounding of the Earth's atmosphere by radio communication links between GPS satellites and hundreds of GPS receivers onboard of telecommunication satellites in low Earth orbit may lead to a nearly complete (and economic) observation of atmosphere dynamics and climate in some future [*Gorbunov*, 1996; *Yunck et al.*, 2000].

[6] Section 2 of our study will present, compare, and discuss observations of global distributions of stratospheric gravity waves at northern and southern midlatitudes as well as the longitudinal variation of lower ionospheric irregularities obtained by the Global Positioning System/Meteorology Experiment (GPS/MET). Accuracy and possible errors of the estimation of stratospheric gravity wave activity from fluctuations of observed temperature profiles have been discussed in detail by *Preusse et al.* [2000] and *Tsuda et al.* [2000]. Then we focus in section 3.1 on the wave activity over Southern Andes which is dominant at southern midlatitudes. Balloon measurements are compared to a nearby GPS/MET temperature profile. Both measurement techni-

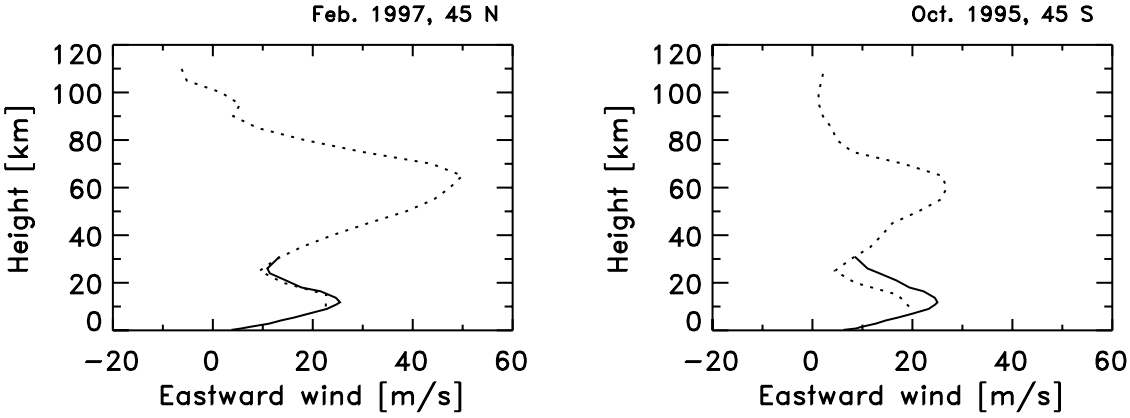

Figure 2. Zonal average of zonal wind as function of height in February 1997 (left-hand-side, geographic latitude 45°N) and October 1995 (right-hand-side, geographic latitude 45°S). Solid lines correspond to zonal wind data provided by NCEP/NCAR reanalysis and Climate Diagnostics Center (CIRES/NOAA) while dotted lines denote predictions of the HWM93 wind climatology.

ques show a similar wave structure which is possibly due to a mountain wave generated by the Andean mountain ridge (section 3.3). The horizontal wind profiles of the balloon observation are used for the determination of the horizontal direction of wave propagation, which is required for analysis and verification of mountain wave propagation up to the stratosphere. The possibility of a wave generation process, different to orographic effect, is carefully checked.

[7] Parallel to GPS/MET and balloon observations of stratospheric wave activity, we analyze the distribution of thin ionization layers (sporadic E) in the lower ionosphere (section 3.2). Neutral wind shears of upward propagating waves from the stratosphere generate thin ionization layers in the lower ionosphere due to an electrodynamical effect of neutral-ion collisions under influence of the geomagnetic field [*Hines*, 1960; *Whitehead*, 1960; *Mathews*, 1998]. These ionization layers are regarded as qualitative tracers of neutral wave activity in the mesosphere/lower thermosphere (MLT region) and are easily detected by GPS radio occultation. Thus GPS radio occultation allows correlative studies on fluctuations in the stratosphere and lower ionosphere, leading to improved knowledge on coupling of stratosphere, MLT region, and lower ionosphere by upward energy and momentum flux of atmospheric waves.

2. Comparison of Atmospheric Fluctuations at Northern and Southern Midlatitudes

2.1. GPS/MET Radio Occultation Data

[8] GPS/MET is a proof-of-concept for accurate profiling of the Earth's atmosphere and ionosphere by GPS radio occultation [*Melbourne et al.*, 1994; *Kursinski et al.*, 1995; *Rocken et al.*, 1997; *Hajj and Romans*, 1998; *Schreiner et al.*, 1999; *Anthes et al.*, 2000]. Fundamentals of the GPS radio occultation technique and recent developments in Earth remote sensing by spaceborne GPS receivers are described in the appendix. The GPS/MET satellite mission has been organized and operated by University Corporation for Atmospheric Research (UCAR) in collaboration with Jet Propulsion Laboratory (JPL) and University of Arizona. The GPS/MET data center at UCAR provides temperature profiles with a vertical resolution of around 1 km. The GPS receiver onboard of the low Earth orbit (LEO) satellite Microlab-1 measures the whole profile of atmospheric refractivity from the orbit height in 735 km down to the surface during a radio occultation. In the present study we only consider GPS/MET data in October 1995 (10 October 1995–25 October 1995) and February 1997 (2 February 1997–11 February 1997) when GPS signal encryption (anti-spoofing) has been turned off, enabling a higher precision of GPS phase measurement. Usually GPS signals are encrypted by the US Department of Defense for prevention of being "spoofed" through the transmission of false GPS signals by an adversary. In average GPS/MET obtained 100–150 temperature profiles per day. Measurement accuracy of absolute temperature is around 1°K or better in the lower stratosphere.

2.2. Mean Wind

[9] The data sets (October 1995 for southern midlatitudes, February 1997 for northern midlatitudes) are around spring and late winter/early spring respectively. As mentioned in the introduction, mean wind can generate atmospheric waves by various processes (e.g., orography, shear flow, jet stream variability) and upward energy/momentum flux of waves with ground-based phase speeds <5 m/s is largely influenced by wave-mean wind interactions.

[10] Monthly averages of the global zonal wind fields in the lower troposphere at 700 mbar are shown in Figure 1 for February 1997 (top) and October 1995 (bottom). Wind data are kindly provided by the NCEP/NCAR reanalysis project in cooperation with NOAA/CIRES Climate Diagnostics Center. Eastward winds are maximal at midlatitudes. At northern midlatitudes there are two strong wind jets ($u > 20$ m/s) over Atlantic and Pacific in February 1997. At southern midlatitudes the eastward wind jet extends around the world. A possible influence/interruption of the wind stream by the southern tip of South America appears in both viewgraphs.

[11] Profiles of average zonal wind at 45°S and 45°N are depicted in Figure 2. The wind profiles show favorable conditions for upward energy/momentum flux of waves, since eastward mean wind is present from the lower atmosphere up to the lower ionosphere. The dotted lines

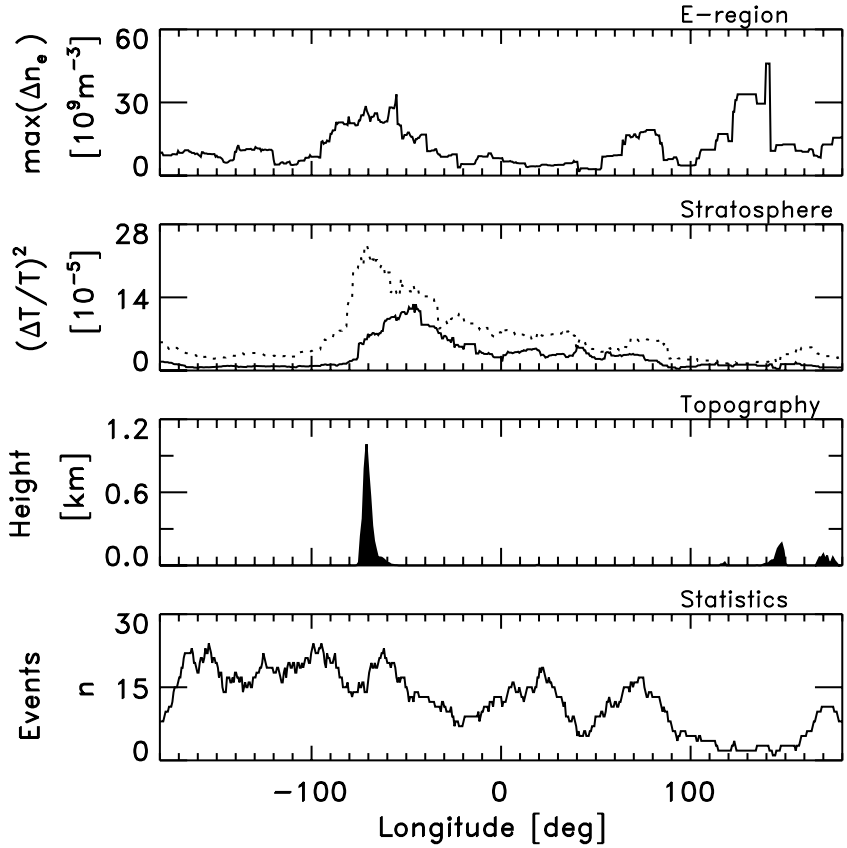

Figure 3. Distributions of occultation events, average topography, average fluctuations in the stratosphere, and E-region at southern midlatitudes (35–55°S) during 10–25 October 1995 (from bottom to top respectively). The solid line of relative temperature variance (vertical wavelengths <7 km) of the stratosphere corresponds to h = 22–28 km, and the dotted line to h = 32–38 km. The sporadic E intensity is estimated by the maximum of electron density variation Δn_e in the height range 80–120 km.

correspond to the rough predictions of the Hedin wind climatology HWM93 [*Hedin et al.*, 1996].

2.3. Fluctuations at Southern Midlatitudes

[12] Here we analyze similarities or possible connections between surface topography, stratospheric GW fluctuations, and sporadic E in the lower ionosphere. For the stratosphere, mean temperature profiles, $\overline{T}$, are estimated by a sliding window average of 7 km in height. The profiles of normalized temperature fluctuations (vertical scales <7 km) are given by $T/\overline{T} = |T - \overline{T}|/\overline{T}$. Recent studies show that GPS/MET profiles of normalized temperature fluctuations are appropriate for investigation of the global distribution of gravity wave activity in the stratosphere [*Preusse et al.*, 2000; *Tsuda et al.*, 2000].

[13] We are starting with the southern hemisphere for 10–25 October 1995. Figure 3 shows from bottom to top panel: the distribution of occultation events within the latitude range 35–55°S, average elevation of the Earth's surface, average variance of normalized temperature fluctuations in the stratosphere (solid line for h = 22–28 km, dotted line for h = 32–38 km), and maximum of electron density variation (vertical scales <7 km) in the lower ionosphere (h = 80–120 km). All curves with exception of the topography are obtained by a sliding window average with a step of 0.6° and a window length of 10° in longitude.

[14] There is an obvious development of the stratospheric wave field from h = 25 km to h = 35 km. Wave activity over Southern Andes increases, and the maximum of wave activity slightly moves westward with increase of height and against the prevailing eastward wind. These characteristics are in agreement with numerous observations and simulations of mountain wave fields [*Gossard and Hooke*, 1975]. It is also remarkable that the temperature variance peak over Andes contains the major part of total stratospheric wave variance at southern midlatitudes in October 1995. Enhanced stratospheric wave activity over Andes has been previously observed by the microwave limb sounding experiment of the Upper Atmosphere Research Satellite [*McLandress et al.*, 2000]. A mountain wave over Andes has been analyzed in detail by means of Crista infra-red limb sounding data [*Eckermann and Preusse*, 1999].

[15] The longitudinal dependence of electron density variation Δn_e (h = 80–120 km) of October 1995 is depicted in the top panel of Figure 3. The retrieval of electron density variations from GPS/MET data has been described by *Hocke and Tsuda* [2001] and *Hocke et al.* [2001]. The fluctuations of the phase path difference profile of GPS L1 and L2 signal are approximately proportional to electron density variations near the ray perigee. We extract variations of vertical scales less than 7 km from the phase path difference profile by the same method as for the temperature profile. Multiplication

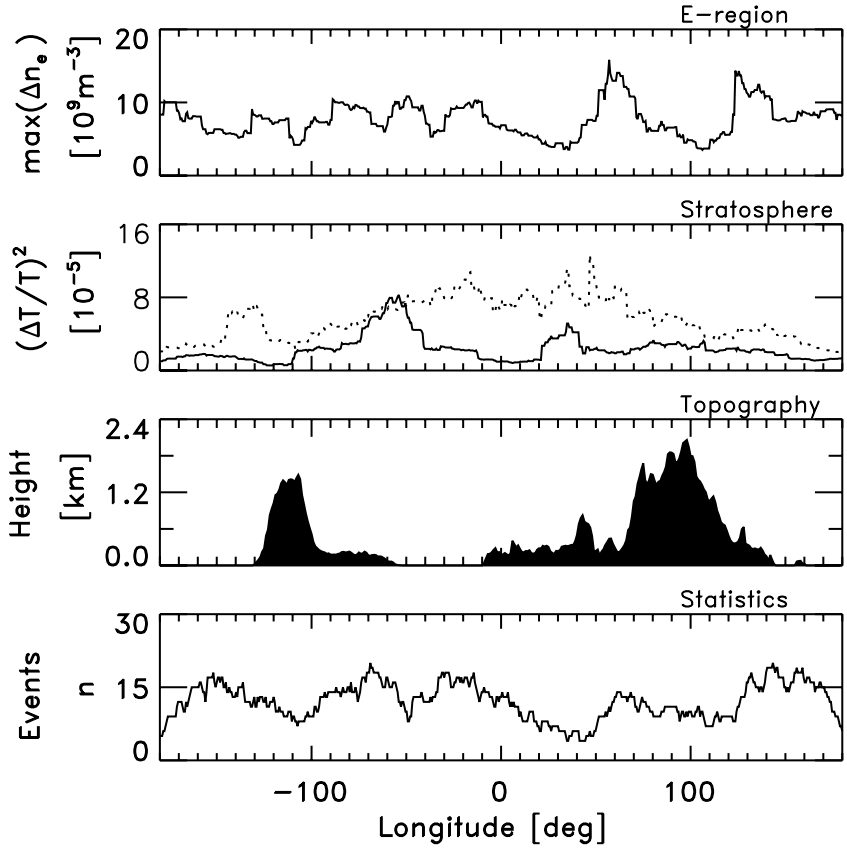

Figure 4. Same as Figure 3, but for the northern hemisphere (35–55°N) during 2–11 February 1997.

by a constant factor yields an estimate of the electron density variations Δn_e with vertical scales less than 7 km [*Hocke and Tsuda*, 2001]. The average Δn_e distribution shows a significant enhancement of sporadic E activity over Andean mountain ridge which could be due to upward propagating, orographic waves from Andes (section 3.2).

[16] There is also a peak of sporadic E, eastward of Australia. The selected latitude range 35° to 55°S includes only the southern part of Australia, and the statistics of GPS/MET occultation events is rather poor in this region, because of gaps of the fiducial GPS ground network which is required for precise phase path determination by double difference method [*Melbourne et al.*, 1994]. However, since we also find enhanced sporadic E over Australia/New Zealand during the other GPS/MET observation times, these ionospheric irregularities could be related to disturbances of the zonal wind flow by the topography of Australia and New Zealand.

[17] In the northern part of Australia, at low latitudes, convectively generated gravity waves due to the high amount of tropospheric water vapor have to be considered [*Hocke and Tsuda*, 2001]. We have looked at the water vapor distribution (GPS/MET and ECMWF water vapor pressure at around h = 5 km) at midlatitudes during February 1997 and October 1995. As expected, we noticed no correlation between stratospheric wave activity and water vapor distribution at midlatitudes for late winter to spring.

2.4. Fluctuations at Northern Midlatitudes

[18] In Figure 4 GPS/MET data of northern midlatitudes are shown during 2–11 February 1997. Topography and background wind of the northern hemisphere are more complex compared to the southern hemisphere. Gravity waves from various sources (e.g., orography, shear flow, jet stream) may overlap incoherently, so that finding of a correlation between tropospheric sources and stratospheric wave activity becomes difficult. Temporal variability of gravity wave flux and considerable travel time of upward propagating wave energy may further prevent the detection of correlations between tropospheric source regions and distributions of stratospheric and ionospheric fluctuations.

[19] The variance of normalized temperature fluctuations at h = 25 km (solid line) shows an increase over North America. There are only a few, weak signatures in the longitudinal distribution of temperature variance suggesting possible orographic effects at northern midlatitudes. Measurements of stratospheric wave activity by *McLandress et al.* [2000] also indicate that there is no clear or simple connection between topography and stratospheric wave activity in the northern hemisphere.

[20] Contrary to the southern hemisphere, the main characteristics of the variance distribution are rapidly changing when waves are propagating from h = 25 km to h = 35 km. The wave field around h = 35 km (dotted line) is increased and has a broad, flat shape. The shape may be described by a sine wave with maximum of wave activity over Europe and minimum over northern Pacific. This finding is in qualitative agreement to long-term observations of the microwave limb sounder of UARS satellite [*McLandress et al.*, 2000, Figure 5d]. The distribution of stratospheric GW fluctuations at northern midlatitudes has probably a

regular climatology, but understanding of its characteristics is more difficult than in case of the southern hemisphere.

[21] The zonal average of temperature variance should be quite similar at northern and southern midlatitudes, if one assumes that gravity wave energy mainly originates from the geostrophic wind. The zonal averages of $(\Delta\overline{T}/T)^2$ are in fact quite similar for Figures 3 and 4. At northern midlatitudes the average of $(T/\overline{T})^2$ is 2.3 10^{-5} at h = 25 km and 5.6 10^{-5} at h = 35 km, while at southern midlatitudes the average of $(T/\overline{T})^2$ is 2.7 10^{-5} at h = 25 km and 6.1 10^{-5} at h = 35 km. The similarity of the zonal averages of temperature variance is remarkable since they originate from quite different longitudinal distributions (narrow peak at southern midlatitudes, broad and flat curve at northern midlatitudes). Further it indicates a consistent measurement of absolute temperature variance by the GPS/MET mission in October 1995 and February 1997.

[22] The distributions of normalized temperature variance at northern and southern midlatitudes show a land/sea contrast where minimal atmospheric wave activity is observed over oceans. At southern midlatitudes, $(\Delta T/\overline{T})^2$ is over a longitude interval of around 180° length (Pacific and Indian Ocean) less than 10^{-5} at h = 25 km (Figure 3). At northern midlatitudes, $(T/\overline{T})^2$ achieves maximal values over the east coast of North America and over Eurasia. Wave activity over Pacific and Atlantic is around 1 to 3 10^{-5} at h = 25 km (Figure 4).

[23] Enhanced wave activity over the east coast of North America is also present in the global map of gravity wave activity in the lower stratosphere of August 1997 in a study by *Preusse et al.* [2001, Figure 1b]. The enhanced wave activity observed by Crista over the east coast of North America, at the west coast of Europe, and westward of Ural has not been discussed by *Preusse et al.* [2001] since the article is focused on convectively generated gravity waves.

[24] In Figure 4 (top), the distribution of lower ionospheric fluctuations shows two maxima, at 60° and at 130°E, where the eastward wind jet over the Pacific begins. The sporadic E distribution over North America shows a periodic variation with a wavelength of around 30–40 degrees in longitude.

3. Orographic Wave Field and Ionospheric Fluctuations Over Andes

3.1. GPS/MET Observations and Results

[25] We concentrate now on the wave field over Andes which is the most remarkable feature of the longitudinal distributions of stratospheric wave activity at midlatitudes. The maximum of temperature variance over Andes at h = 35 km (Figure 3) is around two times greater than the maximum found at northern midlatitudes (Figure 4).

[26] After a long undisturbed way over the Pacific the midlatitude surface wind must pass the Andean mountain ridge. This interaction redistributes energy and momentum from the mean wind field into the "orographic wave field" which is considered here as a superposition of quasi-stationary mountain waves and nonstationary gravity waves of orographic origin with nonzero phase-speed.

[27] Recent satellite observations of MLS and CRISTA show enhanced wave activity in the stratosphere over the southern tip of South America [*Eckermann and Preusse*, 1999; *McLandress et al.*, 2000]. These measurements are in agreement with earlier balloon soundings of the troposphere and lower stratosphere over Mendoza (Argentina) by *de la Torre et al.* [1996]. The temperature and wind velocity profiles of the balloon measurements indicate enhanced wave activity at the tropopause, in around 16 km, and beyond. A possible orographic origin of this wave activity has been suggested by *de la Torre et al.* [1996].

[28] In case of the GPS/MET data of October 1995, the orographic wave field is most obvious when the temperature fluctuation profiles of the latitude range 40 to 55°S are selected. Contrary to the previous section, the profiles include now all temperature fluctuations with vertical scales less than 10 km. The new cut-off wavelength of 10 km (instead of 7 km) is motivated by optimization of the presentation of the wave field over Andes having an apparent vertical wavelength of around 6 km. The main result, enhanced fluctuations over Andes, is also found at other wavelengths, e.g., vertical wavelengths smaller than 5 km or greater than 10 km. In addition, the possible orographic effect of Andes is already visible in the unfiltered temperature profiles (wavy profiles over Andes, smooth profiles over the Pacific).

[29] The selected $\Delta T/\overline{T}$ profiles are averaged by a sliding window of 10° in longitude and a longitude step of 0.6°, so that the $T/\overline{T}$ field is obtained as function of longitude and height. This averaging process enables a rough visualization of the average orographic wave field composed of quasi-stationary mountain waves and nonstationary gravity waves. Quasi-stationary waves—if present—should cause visible structures in the longitude–height section of $\Delta T/\overline{T}$ (e.g., position of nodes), while nonstationary gravity waves of orographic origin possibly cause a broad enhancement of average wave activity around Andes without visible details.

[30] The $\Delta T/\overline{T}$ field is depicted in Figure 5. Obviously the orographic wave field starts at the longitude position of Andean mountain ridge (−73° or 73°W). The response of the temperature fluctuation field at heights below 20 km is small or not measurable. Beyond 20 km the fluctuation amplitude increases, and a vertical wavelength of 6 km is obvious (vertical distances of maxima of absolute fluctuation amplitude correspond to half of the wavelength and are around 3 km in Figure 5). This apparent vertical wavelength of the orographic wave field over Andes agrees with previous observations and theory [*Eckermann and Preusse*, 1999; *Tan and Eckermann*, 2000]. Again, the maximum of the wave field moves slightly westward, against the prevailing eastward wind, with increase of height. The amplitude of the normalized temperature fluctuation is around 2%. Gravity waves with nonzero phase speed may explain broadening and eastward displacements of the average wave field in Figure 5.

3.2. Enhanced Fluctuations of the Lower Ionosphere

[31] In their chapter on mountain waves *Gossard and Hooke* [1975] raise the interesting question if there could be an effect of mountain waves on the ionosphere. Because of insufficient observation data at that time, this question remained unanswered. Numerical simulations of orographic wave fields have now reached upper stratospheric heights, but no simulation has been performed for heights beyond the mesopause [*Tan and Eckermann*, 2000]. *Satomura and Sato* [1999] simulated secondary generation of gravity

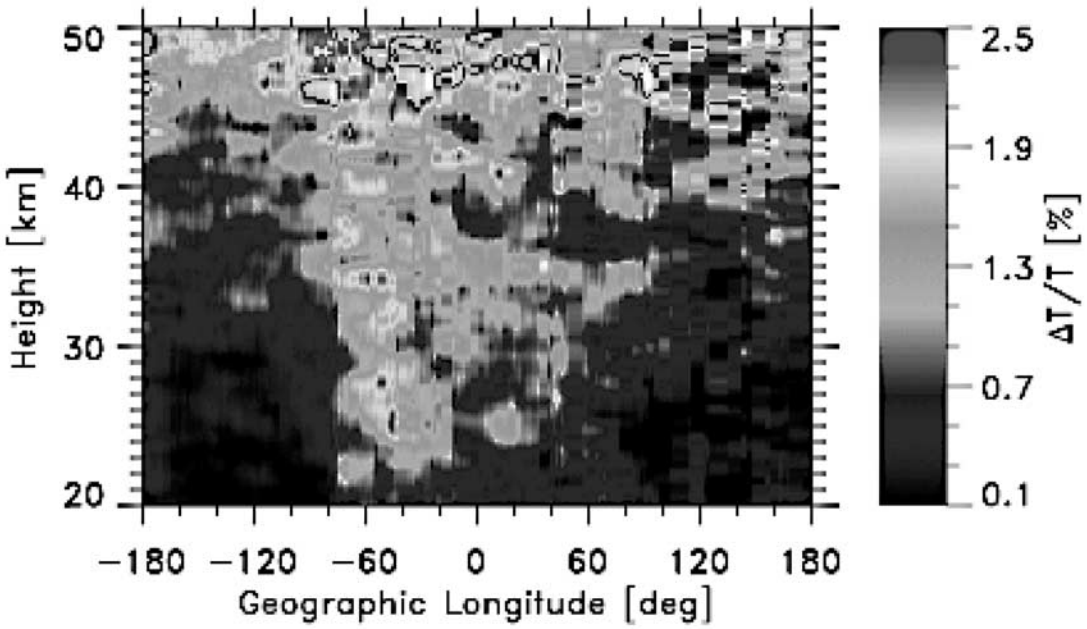

Figure 5. Normalized temperature fluctuations (vertical scales <10 km, $\Delta T/T = |T - \overline{T}|/\overline{T}$) as function of longitude and height for October 1995 at southern midlatitudes (40°–55°S). Vertical wavelength at −70° (70°W) is around 6 km (vertical distances between $T/\overline{T}$ maxima are around 3 km and correspond to the half of the wavelength). See color version of this figure at back of this issue.

waves associated to breaking of mountain waves in the stratosphere. Recently *Meriwether et al.* [1997] observed a horizontal temperature gradient, in zonal direction, in the thermosphere over Andes (at 16°S) and suggested that the temperature variation of around 100–400°K is due to orographic wave heating.

[32] In Figure 3 we already noticed an enhancement of sporadic E over Andes. Now we discuss the longitude–height section of the plasma irregularities Δn_e observed by GPS/MET at southern midlatitudes. The Δn_e field of October 1995 (vertical scales <7 km, latitude range 40 to 55°S) is depicted in Figure 6 as function of longitude and

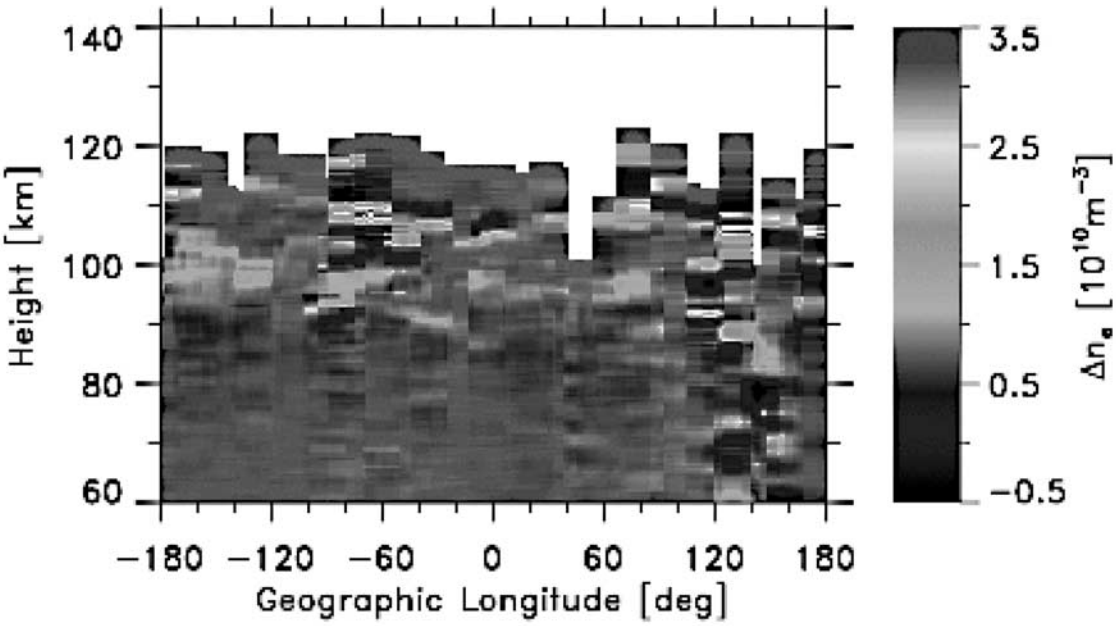

Figure 6. Average plasma density fluctuations (vertical wavelengths less than 7 km) for October 1995 at latitudes 40°–55°S. Around 108 km height and −70° (70°W) a plasma density increase is visible over Andean mountain ridge. Average has been taken with respect to sign of Δn_e. See color version of this figure at back of this issue.

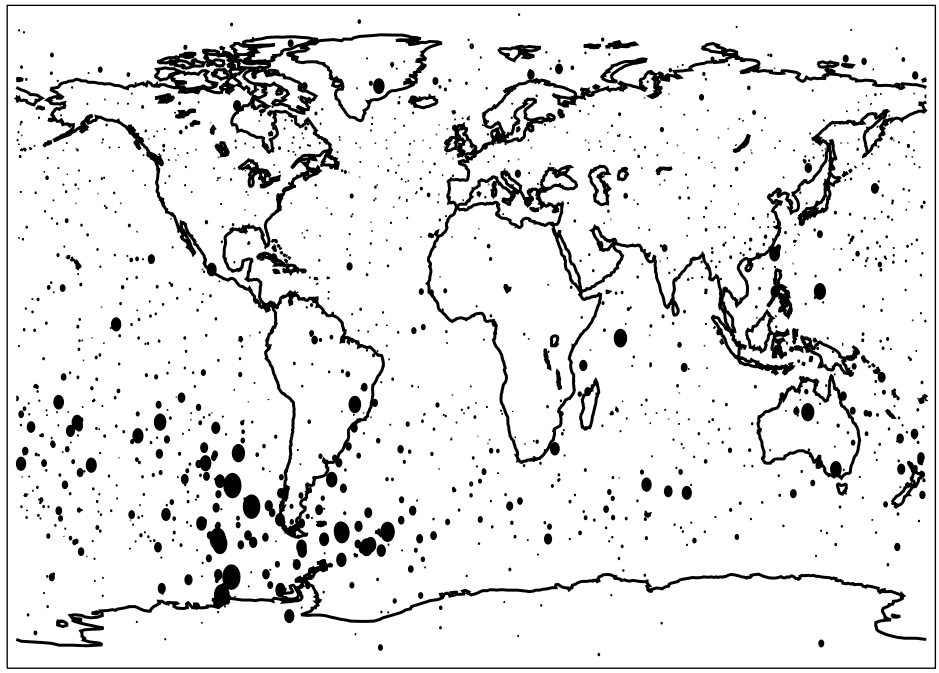

Figure 7. Global map of lower ionospheric irregularities observed by GPS/MET in February 1997. A dot corresponds to a radio occultation event. The dot radius is proportional to the maximal electron density fluctuation (vertical scale <7 km) at heights 90–110 km.

height. The missing GPS/MET data values at the topside are due to the lack of high resolution 50 Hz sampling rate data for ray perigees beyond 120 km height (50 Hz sampling rate corresponds to a ray perigee height step of around 50 m). Statistics of the enhancement at 70°W, h = 108 km, and its vicinity are around 5 events/15 degree (because of the relative large sounding volume of radio occultation measurements, statistics are acceptable). We suggest that this plasma density enhancement is a far-reaching consequence of possible orographic waves from Andes and that it is formed by the wind shear mechanism [*Hines*, 1960; *Whitehead*, 1960]. In the lower ionosphere (dynamo region) neutral winds can induce electric fields, since the motion of ions is coupled by collisions to the neutral wind while the motion of electrons is more influenced by the geomagnetic field. A neutral-wind induced electric field causes a E × B plasma drift, which is upward for eastward wind and downward for westward wind. So the ionospheric plasma is accumulated to thin ionization layers in the nodes of zonal wind shears. Because of recombination processes, sporadic E layers mainly consist of long-living metallic ions [*Mathews*, 1998].

[33] Enhanced sporadic E is also present in the Δn_e field of February 1997 at southern midlatitudes around Southern Andes. Figure 7 shows the world map of Δn_e. Places of all occultations in February 1997 are marked by dots. The dot radius is linear proportional to the maximal Δn_e value observed in the height range 90–110 km. A cluster of large dots shows enhanced electron density fluctuations or sporadic E over the Drake passage between Pacific and Atlantic and South America and Antarctica. Enhanced GW fluctuations are not found in the stratosphere, and contrary to October 1995 an orographic wave field is not present in the GPS/MET observations over Andes. This could be due to prevalent westward mean winds in the stratosphere in February. Orographic waves will then encounter critical levels before reaching the stratosphere. It might be notable that the eastward wind jet at southern midlatitudes (Figure 1) moves southward with increase of height (NCEP/NCAR reanalysis data, not shown here). At lower stratospheric heights the eastward wind jet is exactly centered over the Drake passage between South America and Antarctica, and below the enhanced ionospheric fluctuations of Figure 7. Similar to October 1995, we assume that the cause of the enhanced ionospheric fluctuations in February 1997 are upward propagating waves. An alternative explanation, assuming magnetospheric particle precipitation as cause of sporadic E around Southern Andes, appears unrealistic, since particle precipitation should be enhanced at higher geomagnetic latitudes and at the geomagnetic South Atlantic Anomaly, but not around Southern Andes. Excitation of sporadic E by gravity waves from the southern auroral oval appears unlikely since the Drake passage is located at geomagnetic midlatitudes around 35–40°S. So we only have the idea that the enhanced ionospheric fluctuations in the lower ionosphere around Southern Andes are caused by enhanced upward wave flux from the lower or middle atmosphere, possibly connected to the eastward wind jet and the small passage between Antarctica and South America.

3.3. Rawinsonde Measurements, Mountain Wave Parameters, and Comparison to GPS/MET

[34] In the previous sections atmospheric fluctuations at midlatitudes have been discussed on a global scale and then locally around Andes by means of spaceborne GPS radio occultation. Now in situ measurements of a balloon-borne rawinsonde will provide a complementary description of atmospheric fluctuations over Andes. The balloon observations are compared to a corresponding GPS/MET radio

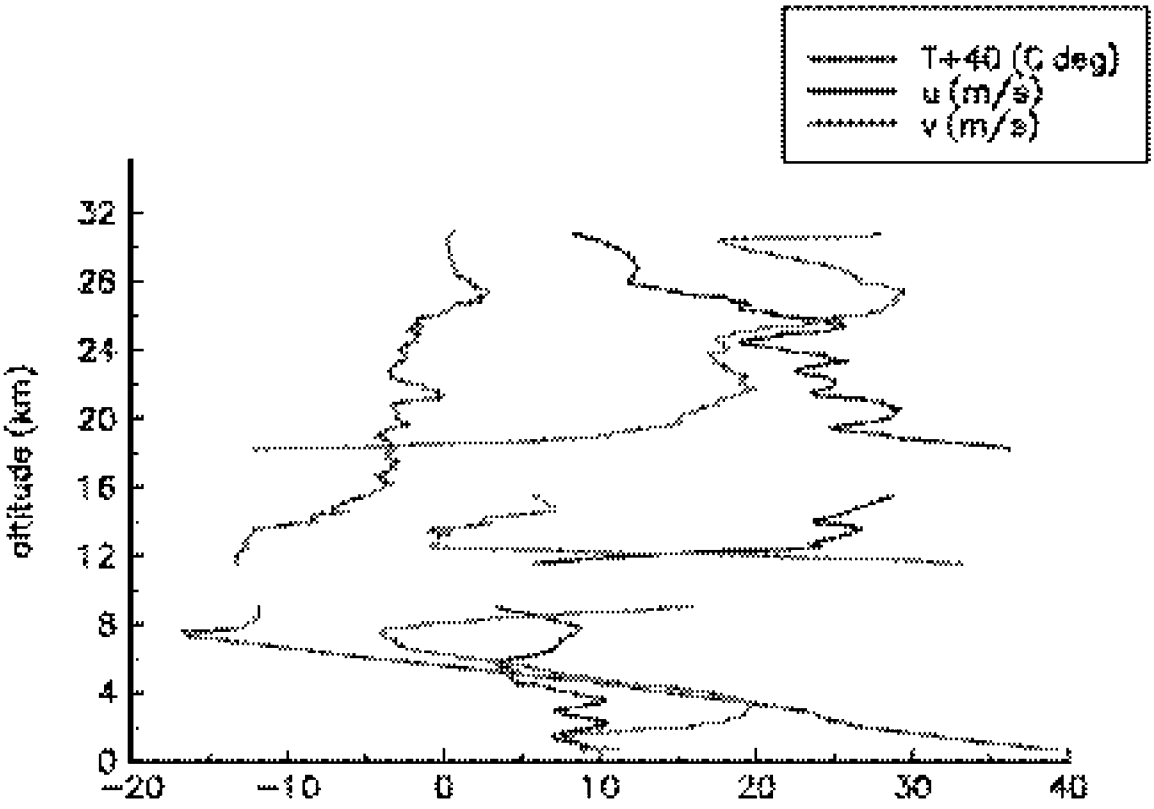

Figure 8. Radiosonde vertical profiles of air temperature T and zonal and meridional wind velocities u and v. Radiosonde launch has been on 24 October 1995 at Ushuaia (54.7°S, 68.1°W). See color version of this figure at back of this issue.

occultation profile over Andes. The atmospheric fluctuations are interpreted by a mountain wave, and several mountain wave parameters are derived from the balloon data. Atmospheric background conditions are investigated to verify a wave generation by orographic effect and to show the possibility of mountain wave propagation from the troposphere to the stratosphere.

[35] Between the end of October and December of 1995, a series of high resolution radiosondes were released from Ushuaia, Argentina, (54.7°S, 68.1°W). The object of that experiment was a study of the atmospheric dynamic conditions in the region, previously to the beginning of a campaign designed to analyze the dynamic and chemical behavior of the southern polar vortex (STRATEOLE experiment [see e.g., *Vial et al.*, 1995]). Regular radiosoundings are not available at the south of Argentina, where Ushuaia is sited. We shall here consider the results from the launching performed on 24 October at 1021 UTC. This is the first one of this radiosonde series. It was selected because it exhibits an interesting signature of a mountain wave and its launching date is within the period considered by the GPS/MET experiment. Each sounding provided high-resolution ($\delta z \approx$ 50 m) profiles of temperature, wind velocity and direction, humidity and altitude. In the case here considered, a maximum altitude of 31 km was attained.

[36] The vertical profiles for the air temperature T and the zonal and meridional wind velocities u and v are shown in Figure 8. Here, a cubic spline converts the irregularly spaced profile into a regular one with a resolution of 50 m. In spite of the two small windows due to missing data in the intervals 9.0–11.5 km (in T, u and v) and 15.5–18.2 (in u and v), a large amplitude oscillation of around 24 m/s peak to peak in v is clearly seen in the troposphere and in the lower stratosphere. We recall that Ushuaia is sited at the south of the southern ''tail'' of the Andes Range. This tail is not aligned in a north-south direction as it is typically the case for the Andes mountains in Argentina, but turns from west to east. From the velocity profiles in Figure 8, the surface wind has at the beginning of the sounding a prevailing northward component. When the sonde had climbed above the mountain tail (with mean altitudes between 1 and 2 km), it slightly turned northward. If this large amplitude oscillation was actually originated by the forcing of these mountains, its high intrinsic frequency character as well as its linear polarization associated to it should be evident by rotating the horizontal frame of reference defined by δu and δv systematically around the vertical direction in small angular steps, projecting δu and δv on the rotated frame at each step. Let us illustrate this idea for a hypothetical single monochromatic wave: after completing a rotation of 180° we should observe at two specific directions say, α and $\alpha + 90°$, only one velocity component, and disappearing the other. At $\alpha + 45°$, both components should be present with identical amplitudes. This would be simply because of the linear polarization of the wave. In our case study, we tested this evidence method for a linearly polarized mountain wave by means of the band-pass filtered δu and δv components. Before the filtering process, the

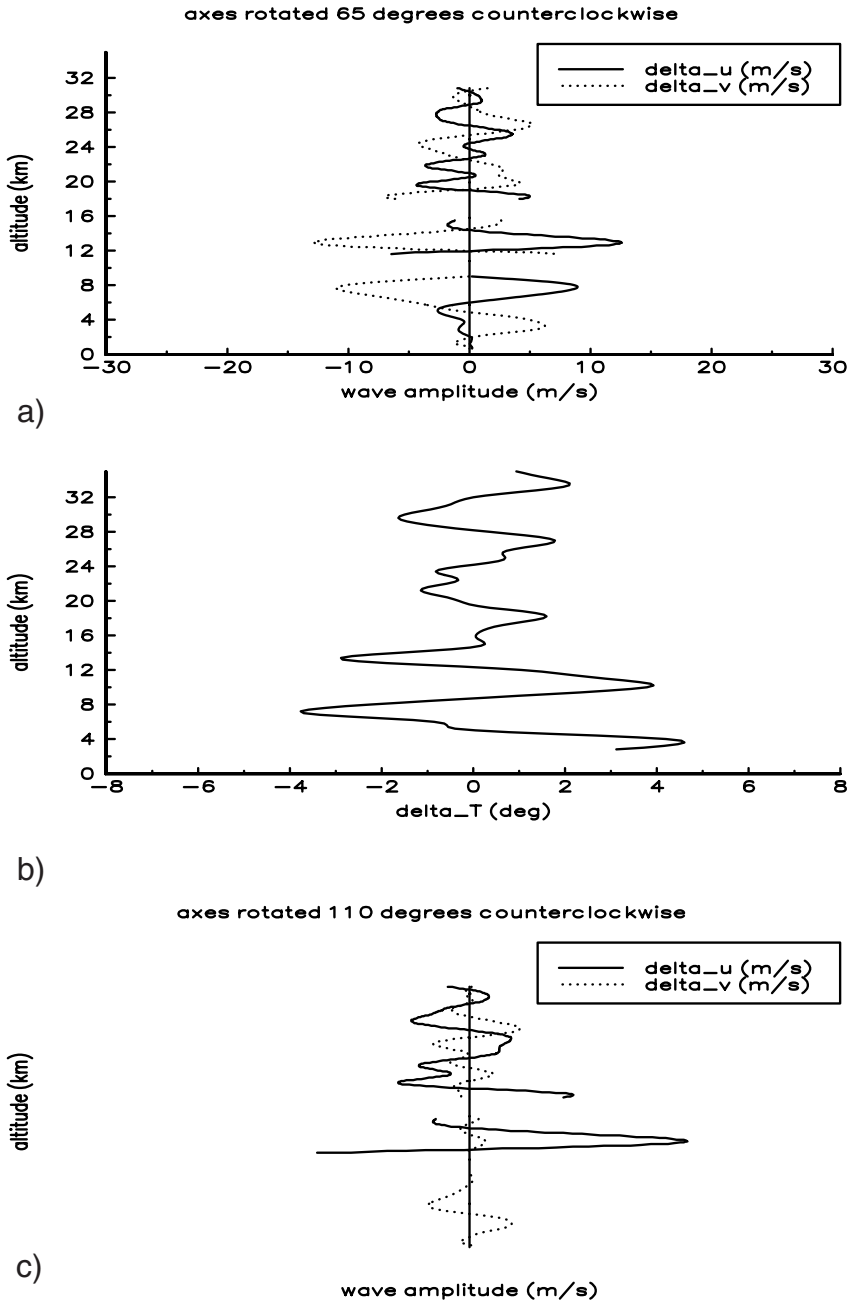

Figure 9. Band-pass filtered radiosonde velocity components from the data shown in Figure 8, projected on an horizontal frame of axes rotated counterclockwise a) 65°, c) 110°, b) band-pass filtered temperature from GPS/MET radio occultation profile.

small data gaps of the u and v profiles have been filled by interpolated values given by the already mentioned cubic spline. A non recursive filter with a band-pass for vertical wavelengths between 2 and 9 km has been applied to isolate each parameter variation from its corresponding mean value. Then, rotating the horizontal axes counterclockwise, the prevailing oscillation in the v profile in Figure 8 diminishes while that in u increases accordingly. Figure 9a shows the band-pass filtered oscillations with respect to a frame rotated counter-clockwise by 65°. Here, an important oscillation with amplitudes near to 10 m/s in each velocity component is present in the troposphere, increasing to around 13 m/s in the lower stratosphere. It suggests that the plane of polarization of the wave, should be here equidistant from both rotated horizontal axes, it is to say, between 65° (direction of the rotated zonal axe) and 175° (direction of the rotated meridional axe) (both angles are taken counterclockwise from east). Then the plane of polarization lies at 110°. δu and δv are here clearly in phase opposition, in agreement with the polarization relations for high frequency gravity waves. Its apparent vertical wavelength is near to 4.5 km. We prefer to distinguish here between apparent and real wavelengths, as far as the atmospheric sounding is not 1) instantaneous nor 2) vertically directed [*de la Torre and*

Alexander, 1995]. The sonde describes an almost constant, low slope trajectory, intersecting consecutive phase surfaces "prematurely". This happens due to the high slope of phase surfaces associated with a high intrinsic frequency wave. Then, the apparent vertical wavelength detected with a radiosonde must be expected to be shorter than the real one. Only in a pure vertically directed radiosounding, apparent (it is to say, measured) and real wavelengths would coincide between themselves for zero phase velocity waves.

[37] The apparent vertical wavelength detected with radiosondes must be expected to be shorter than the real ones. We performed the same band-pass filtering process above described on the temperature profile obtained from the GPS/MET experiment on 24 October 1995 (52°S, 65°W), at the north-east of the Andes tail and near to the region crossed by the radiosonde (Figure 9b). A large amplitude oscillation is clear below 15 km, with a vertical wavelength near to 6 km. This vertical wavelength is observed as a real one. Between 10 and 25 km the resembling of the general features of the profiles obtained by radiosonde and GPS exhibits a striking similarity, though the data are not sufficient to prove that radiosonde and GPS observed indeed the same mountain wave. For this purpose a perfect coincidence in time and place of radiosonde and GPS is required, and effects of the GPS sounding volume on the measurement result have to be considered (appendix). The vertical wavelength of the individual occultation event on 24 October (Figure 9b) is in agreement to that of the average orographic wave field (10–25 October) depicted in Figure 5. The vertical wavelength is larger than the apparent wavelength detected with the radiosonde, as expected. The difference between real and apparent wavelength oscillations provides additional information about the wave detected. In fact, for high intrinsic frequency stationary waves (nonhydrostatic regime) the tilt of phase surfaces and therefore the discrepancy between real and apparent wavelengths will be larger than for inertial waves. In this last case the discrepancy is usually negligible for any radiosonde trajectory, as the phase surfaces are close to horizontal. Figure 9c represents another position of the horizontal frame rotation, now corresponding to 110°. It may be observed the prevailing δu component near to 15 and 20 m/s in the troposphere and the lower stratosphere respectively, while δv has been considerably reduced. Thus we interpret the balloon measurements by a linearly polarized gravity wave of large amplitude and high intrinsic frequency having a horizontal direction of propagation to 110° counterclockwise from east (approximately NNW). Above the lower stratosphere, the wave amplitude obtained from the radiosounding diminishes (Figures 9a and 9c) while preserving a phase difference of 0 or π rad between both components. This reduced amplitude is observed in the GPS/MET profile too (Figure 9b). The calculated ascent rate also exhibits an important large amplitude oscillation of 2 m/s superposed on the mean ascent rate of around 5–6 m/s in the troposphere (not shown here), as expected for the vertical velocity amplitude of high frequency intense mountain waves and with the same apparent vertical wavelength already observed in δu and δv.

[38] The ECMWF (European Center Medium-Range Weather Forecast) analyses data from 24 October 1995, 0600 UTC and 1200 UTC at the level 925 hPa are shown in Figure 10. The presence of intense winds blowing almost normally to the Andes Range (south of latitude 50°S) is obvious. Both from radiosonde data and from GPS/MET data obtained on that day slightly at the north-east from Ushuaia, the same large amplitude mountain wave event could have been detected. By means of further ECMWF reanalysis data we have looked for possible evidence of other sources of high frequency waves different from mountain waves in the region, in particular, front systems, convection, jet streams, wind shears, and wind amplification. Temperature maps from ECMWF at different levels between 1000 and 150 hPa (not shown here) do not exhibit any front near to Ushuaia, in the region limited by latitudes 50°S and 55°S and longitudes 70°W and 65°W. Only at 300 hPa but at the east of this zone, a front displacing slowly eastward is observed. NOAA satellite infrared images show some cloud systems around Ushuaia on that day and the humidity profile obtained from the radiosonde exhibit an increase at low heights, but we do not see any trace of strong convection processes deserving to be taken into account. Jet streams are neither observed in the region between 1000 and 150 hPa.

[39] We now consider, as generally accepted [see e.g., *Gill*, 1982], that three main factors could influence this mountain-wave propagation up into the stratosphere as well as its momentum deposition: critical layers absorption, trapping and reflection. The possible contribution of each mechanism must be evaluated. In the altitude interval of this sounding, the flux is stable as far as the calculated Richardson number $Ri = N^2/(dU/dz)^2$ is always greater than 0.25, where N is the buoyancy frequency and U is the horizontal wind. This does not depend upon the smoothing chosen for U and N. Generally speaking, under this condition the mountain wave may encounter critical levels and being absorbed or reflected if its propagation is i) vertical or ii) horizontal (trapped wave). From Figure 8, it is clear that zero wind levels are not found throughout the sounding. Furthermore, the only feature observed in the potential temperature gradient $d\theta/dz$ (Figure 11a) is the usual change in slope around the tropopause. Isentropic layers (zero gradient) indicating critical layers are not present. It must be noted that the upstream tilt of mountain waves assures that the radiosonde always crosses leeward consecutive wave phase surfaces. This minimizes the possibility that the trajectory of the balloon would describe path segments parallel to phase surfaces, so detecting apparent zero vertical gradient layers of potential temperature. Then, in the absence of critical levels, the mountain wave may propagate vertically depending on

$$m^2 = l^2 - k^2, \tag{1}$$

where m and k are the horizontal and vertical wave numbers and l^2 is the Scorer parameter, defined as

$$l^2(z) = \frac{N^2(z)}{U^2(z)} - \frac{d^2U(z)/dz^2}{U(z)}. \tag{2}$$

Here, $U(z)$ represents the horizontal velocity profile in the direction of wave propagation, which has been detected above. If m^2 changes abruptly at a given height, a partial reflection for the upward propagating mountain wave takes place. It would be total reflection if m^2 vanishes at a given altitude and negative anywhere above it (trapping effect). In

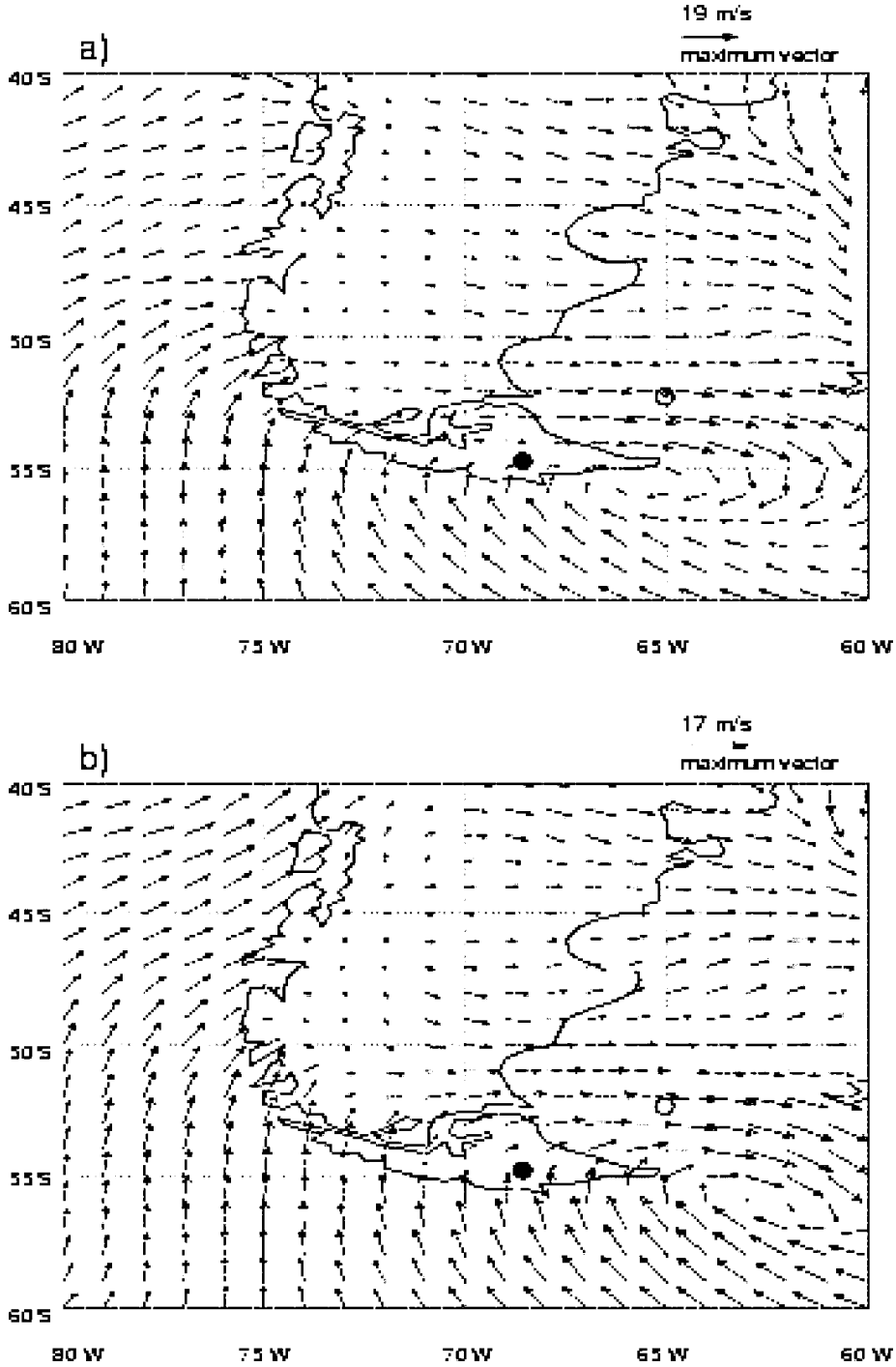

Figure 10. Mean wind at 925 hPa, a) 0600 UTC and b) 1200 UTC, 24 October 1995, from the analyses of the European Center for Medium-Range Weather Forecasts (ECMWF). Full circle denotes the launch place of the balloon. The ascending balloon travels with the wind towards the GPS radio occultation place (open circle). Horizontal displacement of the balloon is around 4–5 times greater than the corresponding vertical displacement.

the calculation of l^2 shown in Figure 11b, the horizontal projection of the wave vector obtained above, at 110° counter-clockwise from the East was used to obtain the U profile along this direction. The main features in Figure 11b does not depend upon the smoothing low-pass filtering applied to $U(z)$ before the calculation of l^2. It may be observed that this parameter is always atypically large along the sounding. Between 0 and 31 km height, its minimum value is 2.0 10^{-6} rad/m^2. Any wave with horizontal wave number less than this value would be free of suffering possible leaking and/or trapping effects. This lower limit allows the propagation of a wave with horizontal wavelength greater than 4.4 km. This value does not suppose important restrictions to currently measured nonhydrostatic

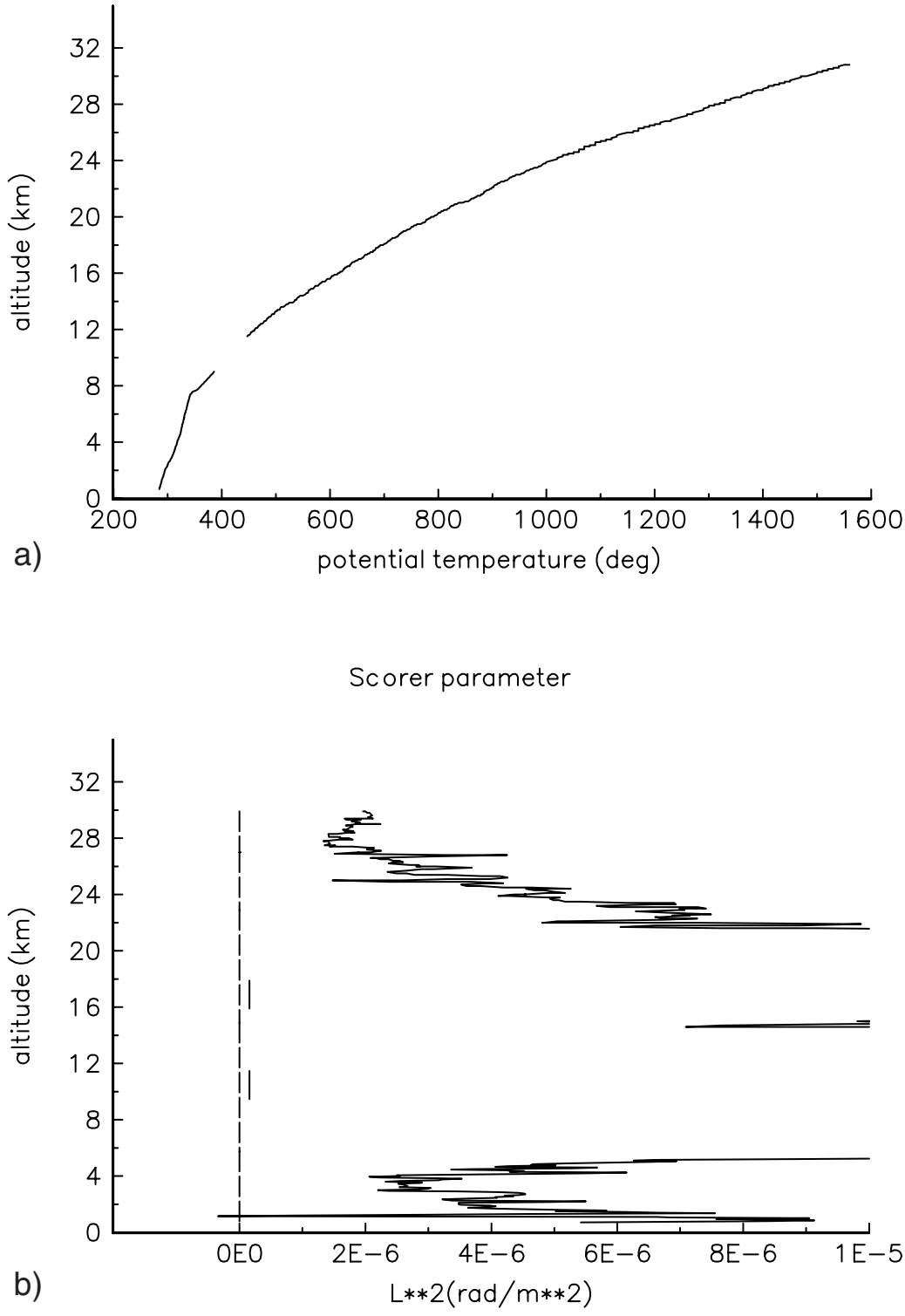

Figure 11. Conditions for mountain wave propagation: a) Potential temperature profile calculated from the radiosonde, b) Scorer parameter calculated from the radiosonde data (see text).

mountain waves. However, the strong variation of l^2 with height could be responsible for some energy absorption and the consequent decrease in wave amplitude observed there both in the sounding and in the occultation profiles. *Schoeberl* [1985] had pointed out that mountain waves are able to propagate up to the stratosphere and even to the mesosphere in the absence of zero mean wind levels in steady mean atmosphere. Even if zero wind level are found a non steady case would also allow mountain waves to reach these high altitudes [*Lott and Teitelbaum*, 1993]. In our case study, from the data from ECMWF at 0600 and 1200 UTC and from the radiosounding, we see that we have

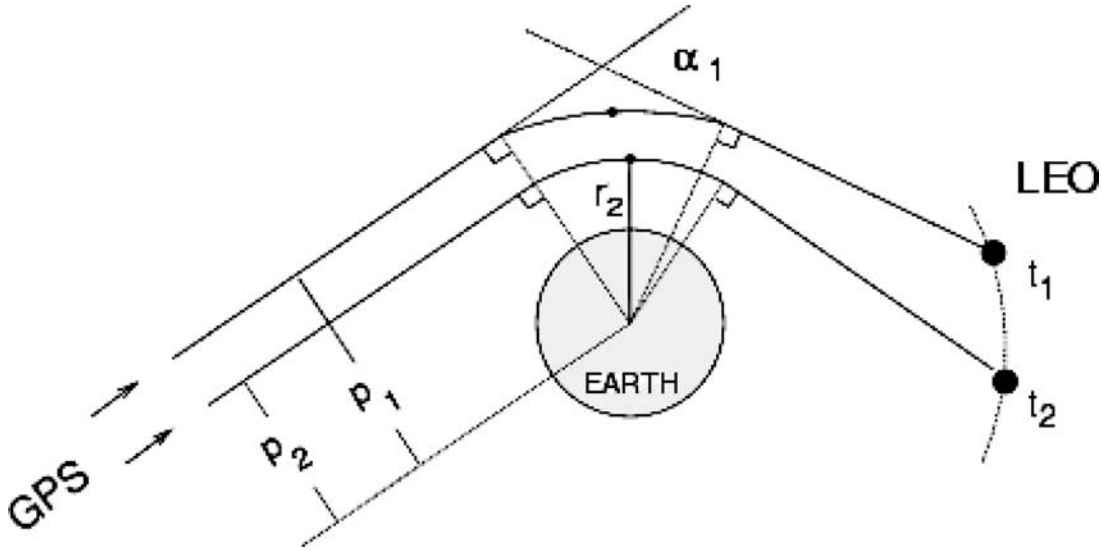

Figure 12. Scheme of radio occultation technique. Radio rays originating from a GPS satellite in around 20,000 km distance are refracted by the earth's atmosphere. A GPS receiver onboard of a low earth orbit satellite (LEO, e.g., in 1000 km height) measures the bending angle α_1 of the ray with impact parameter p_1 at time t_1. Measurement configuration is quite similar to those of particle scatter experiments in physics.

here a case which is: i) steady, and ii) with no zero wind levels. This reinforce the conclusion of a mountain wave signature propagating up to high levels into the stratosphere.

4. Concluding Remarks

[40] The global distributions of stratospheric GW fluctuations and lower ionospheric irregularities at midlatitudes have been analyzed by means of GPS radio occultation. It is found that the zonal average of normalized temperature variance (vertical scales <7 km) is quite similar for northern and southern midlatitudes, though the longitudinal dependences of temperature variance essentially differ. At southern midlatitudes stratospheric GW activity has a strong peak over Andes while at northern midlatitudes GW activity has a broad and flat distribution, probably due to more complex topography and background winds. Remarkable is a rapid change of the temperature variance distribution at northern midlatitudes between 25 and 35 km height. However, the main characteristics of the temperature variance distributions at midlatitudes observed by the new GPS/MET radio occultation technique are in agreement to previous long-term observations by the microwave limb sounder on UARS [*McLandress et al.*, 2000].

[41] At southern midlatitudes, signatures of an orographic wave field with an apparent vertical wavelength of around 6 km are detected in the stratosphere over Andes. Intensity of the wave field increases with height, while its intensity maximum moves westward against the prevailing wind. Previous observation and analysis of a mountain wave with a vertical wavelength of around 6 km in the stratosphere (h = 15–45 km) over Andes by CRISTA [*Eckermann and Preusse*, 1999] further support our interpretation of the GPS/MET observations by an orographic wave field composed of quasi-stationary mountain waves and nonstationary gravity waves of orographic origin.

[42] Thin ionization layers (sporadic E) are found to be increased over Andes and may indicate enhanced orographic wave flux due to the Andean mountain ridge. A correlation between stratospheric GW fluctuations and lower ionospheric irregularities has already been observed for the atmosphere over tropical convection zones [*Hocke and Tsuda*, 2001] and indicates a coupling of lower, middle, and upper atmosphere by upward energy and momentum flux of waves.

[43] The analysis of simultaneous measurements of a balloon radiosonde launched from the southern tip of the Andes Range indicates a large amplitude mountain wave propagating up to the stratosphere. The radiosonde data are interpreted by a linearly polarized mountain wave of high intrinsic frequency propagating in NNW direction. Additionally we have found favorable background conditions for mountain wave generation and propagation in October 1995. No evidence for other possible wave generation mechanisms such as weather front, convective clouds, or jet stream variability has been noticed for the place and date of the radiosonde launch.

[44] GPS radio occultation seems to be a valuable observation technique for finding of atmospheric wave sources and recognition of the dynamic connection between lower, middle, and upper atmosphere. GPS limb sounding of the lower ionosphere with a high sampling rate (10–100 Hz) opens new possibilities for atmospheric research. For further exploration of GPS radio occultation, results and experiences of ground-based remote sensing and in situ measurements are valuable as well as comparative studies with other remote sensing techniques from space.

Appendix: Radio Occultation Technique

[45] For over 30 years the radio occultation technique has been used to sound planetary atmospheres and ionospheres

[*Fjelbo et al.*, 1971]. The measurement principle is based on the bending of radio waves due to atmospheric refraction and on the concept of bistatic radar. The measurement configuration is illustrated in Figure 12 for radio occultation links between a GPS and a low Earth orbit (LEO) satellite. The deviation of the radio signal path from the straight line vacuum path is called atmospheric phase path excess. The phase path excess is calculated by using precise satellite positions (ephemerides) and GPS phase path data recorded by a GPS receiver onboard of the LEO satellite. The phase path excess is closely related to the atmospheric bending angle α (for all necessary formulas we refer the reader to *Melbourne et al.* [1994] and *Kursinski et al.* [2000]). In reality the observed bending angles are much smaller than in Figure 12. Maximal bending angles α are around $1-2°$ for rays close to the Earth's surface and decrease exponentially with height. Measurement accuracy of bending angles can be of order 10^{-4} to 10^{-5} degree.

[46] Each time a GPS satellite rises or sets on the horizon as viewed by the LEO satellite, the signal path slices nearly vertically through the atmosphere, and a profile of atmospheric bending angle α as function of impact parameter p can be derived from the observed time series of phase path excess (Figure 12). The term ''impact parameter'' originates from classical mechanics. Within a radial refractivity field $N(r)$, the trajectory of a GPS photon (GPS signal) with a given impact parameter is determined by conservation of angular momentum. The ray perigee (point of closest approach) of, for example, the second ray trajectory in Figure 12 is at radial distance $r_2 = p_2/\mu(r_2)$ where $\mu(r_2) = 1 + N(r_2)\ 10^{-6}$ the refractive index is. Assuming spherical symmetry of the atmosphere along the ray path, the bending angle profile is inverted into a refractivity profile by the Abel inversion [*Fjeldbo et al.*, 1971]. The refractivity profile represents an average over an effective atmospheric sounding volume centered around the ray perigee at the Earth's limb. The sounding volume is similar to a tube with a length of less a few hundreds kilometers and a diameter of around 1 km. The resolution of radio occultation may be roughly estimated by 1 km in vertical and 100 km in horizontal direction. This does not imply that radio occultation is insensitive to atmospheric waves of smaller horizontal wavelengths. If the radio ray is parallel to a horizontal phase front of a gravity wave, then horizontal wavelengths less than 100 km are detectable. *Jiang and Wu* [2001] discuss this effect of aspect sensitivity for passive limb sounding of gravity waves in the Arctic vortex.

[47] Similar to radars, radio occultation is sensitive to small-scale structures which cause constructive and destructive interference of the scattered radio signals (in principle all atmospheric structures greater than the radio wavelength can cause phase and amplitude scintillations of the received radio signal). In so far the previous estimation of resolution of radio occultation has been misleading, since a detailed analysis of radio scintillations observed during a radio occultation can inform about much smaller scales in a statistical manner. Retrieval of average properties of small-scale irregularities (100 m to a few kilometer) requires the calculation of a theoretical radio scintillation spectrum for a model spectrum of atmospheric irregularities by means of weak scattering theory and phase screen approach. The best fit of a theoretical spectrum of radio scintillations to the observed radio scintillation spectrum yields the power spectrum of atmospheric irregularities, axial ratios of irregularities, and direction of anisotropy [*Hinson and Tyler*, 1983].

[48] The refractivity profile is linear proportional to the electron density profile of the ionosphere at heights beyond 60 km. At heights between the upper troposphere and 50 km the refractivity profile is linear proportional to the neutral density profile. By means of hydrostatic equilibrium and equation of state the neutral density profile First yields the pressure and then the temperature profile. Validation studies of GPS radio occultation experiments indicated a temperature retrieval error of around 1 Kelvin or less in the lower stratosphere [*Rocken et al.*, 1997]. By means of improved GPS antenna/receiver systems such as onboard of the CHAMP satellite this accuracy can be attained for both GPS anti-spoofing on and off, allowing continuous and precise monitoring of the atmosphere [*Wickert et al.*, 2001]. In the lower troposphere the additional refraction of the GPS signal by water vapor has to be considered for optimal estimation of temperature, density, pressure, and water vapor pressure from the observed refractivity [*Healy and Eyre*, 2000].

[49] Combination of GPS radio occultation and the rather new GPS reflection technique may provide a measurement tool for global observation of the interaction between ocean, atmosphere, and ionosphere [*Pavelyev et al.*, 1996; *Komjathy et al.*, 1999; *Zavarotny and Voronovich*, 2000; *Beyerle and Hocke*, 2001]. High precision ephemerides of LEO satellites allow recovery of temporal and spatial deviations of the Earth's gravity field, for example, due to global mass transports by ocean, atmosphere, and ice [*Chao et al.*, 2000].

[50] **Acknowledgments.** We thank A. Pavelyev for his advice on ionospheric behavior over ocean and land. We are grateful to C. Rocken and to the GPS/MET teams at UCAR and JPL for data (http://www.cosmic. ucar.edu/gpsmet). N. Balan and H. Takahashi are thanked for discussions. Atmospheric wind data have been provided by ECMWF (UK) and Climate Diagnostics Center at CIRES/NOAA (http://www.cdc.noaa.gov/Composites/); topography data are from NCAR (Boulder). This study was supported by the Japanese GPS-Meteorology project of the Ministry of Education, Culture, Sports, Science, and Technology. A. de la Torre was supported by UBA grant TX-40. K. Hocke was partly supported by Telecommunications Advancement Organization of Japan. We thank the reviewers for their time, efforts, and advices.

References

Alexander, M. J., Interpretations of observed climatological patterns in stratospheric gravity wave variance, *J. Geophys. Res.*, *103*, 8627–8640, 1998.

Alexander, M. J., and R. A. Vincent, Gravity waves in the tropical lower stratosphere: A model study of seasonal and interannual variability, *J. Geophys. Res.*, *105*, 17,983–17,993, 2000.

Anthes, R. A., C. Rocken, and Y.-H. Kuo, Applications of COSMIC to meteorology and climate, *Terr. Atmos. Ocean. Sci.*, *11*, 115–156, 2000.

Beyerle, G., and K. Hocke, Observation and simulation of direct and reflected GPS signals in radio occultation experiments, *Geophys. Res. Lett.*, *28*, 1895–1898, 2001.

Chao, B. F., E. C. Pavlis, C. Hwang, C.-C. Liu, C. K. Shum, C.-L. Tseng, and M. Yang, COSMIC: Geodetic applications in improving earth's gravity model, *Terr. Atmos. Ocean. Sci.*, *11*, 365–378, 2000.

de la Torre, A., and P. Alexander, The interpretation of wavelengths and periods as measured from atmospheric balloons, *J. Appl. Meteorol.*, *34*, 2747–2756, 1995.

de la Torre, A., H. Teitelbaum, and F. Vial, Stratospheric and tropospheric wave measurements near the Andes mountains, *J. Atmos. Terr. Phys.*, *58*, 521–530, 1996.

Eckermann, S. D., and P. Preusse, Global measurements of stratospheric mountain waves from space, *Science*, *286*, 1534–1537, 1999.

Fetzer, E. J., and J. C. Gille, Gravity wave variance in LIMS temperatures, 1, Variability and comparison with background winds, *J. Atmos. Sci.*, *51*, 2461–2483, 1994.

Fjeldbo, G., A. J. Kliore, and V. R. Eshleman, The neutral atmosphere of Venus as studied with the Mariner V radio occultation experiments, *Astron. J.*, *76*, 123–140, 1971.

Fritts, D. C., and G. D. Nastrom, Sources of mesoscale variability of gravity waves, 2, Frontal, convective, and jet stream excitation, *J. Atmos. Sci.*, *49*, 111–127, 1992.

Gill, A. E., *Atmosphere–Ocean Dynamics*, Academic, San Diego, Calif., 1982.

Gorbunov, M. E., Three-dimensional satellite refractive tomography of the atmosphere: A numerical simulation, *Radio Sci.*, *31*, 95–104, 1996.

Gossard, E. E., and W. H. Hooke, *Waves in the Atmosphere*, p. 457, Elsevier Sci., New York, 1975.

Hajj, G. A., and L. J. Romans, Ionospheric electron density profiles obtained with the Global Positioning System: Results from the GPS/MET experiment, *Radio Sci.*, *33*, 175–190, 1998.

Healy, S. B., and J. R. Eyre, Retrieving temperature, water vapour and surface pressure information from refractive-index profiles derived by radio occultation: A simulation study, *Q. J. R. Meteorol. S.*, *126*, 1661–1684, 2000.

Hedin, A. E., et al., Empirical wind model for the upper, middle amd lower atmosphere, *J. Atmos. Sol. Terr. Phys.*, *58*, 1421–1447, 1996.

Hines, C. O., Internal gravity waves at ionospheric heights, *Can. J. Phys.*, *38*, 1441–1481, 1960.

Hinson, D. P., and G. L. Tyler, Internal gravity waves in Titan's atmosphere observed by Voyager radio occultation, *Icarus*, *54*, 337–352, 1983.

Hocke, K., and T. Tsuda, Gravity waves and ionospheric irregularities over tropical convection zones observed by GPS/MET radio occultation, *Geophys. Res. Lett.*, *28*, 2815–2818, 2001.

Hocke, K., K. Igarashi, M. Nakamura, P. Wilkinson, J. Wu, and J. Wickert, Global sounding of sporadic E layers by the GPS/MET experiment, *J. Atmos. Sol. Terr. Phys.*, *63*, 1973–1980, 2001.

Jiang, J. H., and D. L. Wu, UARS MLS observations of gravity waves associated with the Arctic winter stratospheric vortex, *Geophys. Res. Lett.*, *28*, 527–530, 2001.

Komjathy, A., J. L. Garrison, and V. Zavorotny, GPS: A new tool for ocean science, *GPS World*, *4*, 50–56, 1999.

Kursinski, E. R., G. A. Hajj, K. R. Hardy, L. R. Romans, and J. T. Schofield, Observing tropospheric water vapor by radio occultation using the global positioning system, *Geophys. Res. Lett.*, *22*, 2365–2368, 1995.

Kursinski, E. R., G. A. Hajj, S. S. Leroy, and B. Herman, The GPS radio occultation technique, *Terr. Atmos. Ocean. Sci.*, *11*, 53–114, 2000.

Lott, F., and H. Teitelbaum, Topographic waves generated by a transient wind, *J. Atmos. Sci.*, *50*, 2607–2624, 1993.

Mathews, J. D., Sporadic E: Current views and recent progress, *J. Atmos. Sol. Terr. Phys.*, *60*, 413–435, 1998.

McLandress, C., M. J. Alexander, and D.-L. Wu, Microwave limb sounder observations of gravity waves in the stratosphere: A climatology and interpretation, *J. Geophys. Res.*, *105*, 11,947–11,962, 2000.

Melbourne, W. G., E. S. Davis, C. B. Duncan, G. A. Hajj, K. R. Hardy, E. R. Kursinski, T. K. Meehan, and L. E. Young, The application of spaceborne GPS to atmospheric limb sounding and global change monitoring, *JPL Publ. 94-18*, Jet Propul. Lab., Pasadena, Calif., 1994.

Meriwether, J. W., M. A. Biondi, F. A. Herrero, C. G. Fesen, and D. C. Hallenback, Optical interferometric studies of the nighttime equatorial thermosphere: Enhanced temperatures and zonal wind gradients, *J. Geophys. Res.*, *102*, 20,041–20,058, 1997.

Murayama, Y., T. Tsuda, and S. Fukao, Seasonal variation of gravity wave activity in the lower atmosphere observed with the MU radar, *J. Geophys. Res.*, *99*, 23,057–23,069, 1994.

Nastrom, G. D., and D. C. Fritts, Sources of mesoscale variability of gravity waves, 1, Topographic excitation, *J. Atmos. Sci.*, *49*, 101–110, 1992.

Pavelyev, A. G., A. V. Volkov, A. I. Zakharov, S. A. Krutikh, and A. I. Kucherjavenkov, Bistatic radar as a tool for earth investigation using small satellites, *Acta Astronaut.*, *39*, 721–730, 1996.

Preusse, P., S. D. Eckermann, and D. Offermann, Comparison of global distributions of zonal-mean gravity wave variance inferred from different satellite instruments, *Geophys. Res. Lett.*, *27*, 3877–3880, 2000.

Preusse, P., G. Eidmann, S. D. Eckermann, B. Schaeler, R. Spang, and D. Offermann, Indications of convectively generated gravity waves in Crista temperatures, *Adv. Space Res.*, *27*, 1653–1658, 2001.

Rocken, C., et al., Analysis and validation of GPS/MET data in the neutral atmosphere, *J. Geophys. Res.*, *102*, 29,849–29,866, 1997.

Sato, K., Small-scale wind disturbances observed by the MU radar during the passage of Typhoon Kelly, *J. Atmos. Sci.*, *50*, 518–537, 1993.

Satomura, T., and K. Sato, Secondary generation of gravity waves associated with the breaking of mountain waves, *J. Atmos. Sci.*, *56*, 3847–3858, 1999.

Schoeberl, M. R., The penetration of mountain waves into the middle atmosphere, *J. Atmos. Sci.*, *42*, 2856–2864, 1985.

Schreiner, W. S., S. V. Sokolovskiy, C. Rocken, and D. C. Hunt, Analysis and validation of GPS/MET radio occultation data in the ionosphere, *Radio Sci.*, *34*, 949–966, 1999.

Tan, K.-A., and S. D. Eckermann, Numerical simulation of mountain waves in the middle atmosphere over South Andes, in *Atmospheric Science Across the Stratopause*, *AGU Monogr. Ser.*, vol. 123, edited by D. E. Siskind, S. D. Eckermann, and M. E. Summers, pp. 311–318, AGU, Washington D. C., 2000.

Tsuda, T., M. Nishida, C. Rocken, and R. H. Ware, A global morphology of gravity wave activity in the stratosphere revealed by the GPS occultation data (GPS/MET), *J. Geophys. Res.*, *105*, 7257–7273, 2000.

Vial, F., et al., STRATEOLE: A project to study Antarctic polar vortex dynamics and its impact on ozone chemistry, *Phys. Chem. Earth*, *20*, 83–96, 1995.

Vincent, R. A., and M. J. Alexander, Gravity waves in the tropical lower stratosphere: An observational study of seasonal and interannual variability, *J. Geophys. Res.*, *105*, 17,971–17,982, 2000.

Wickert, J., C. Reigber, G. Beyerle, R. König, C. Marquardt, T. K. Meehan, W. G. Melbourne, and K. Hocke, Atmosphere sounding by GPS radio occultation: First results from CHAMP, *Geophys. Res. Lett.*, *28*, 3263–3266, 2001.

Whitehead, J. D., Formation of the sporadic E layer in the temperate zones, *Nature*, *188*, 567, 1960.

Yunck, T. P., C.-H. Liu, and R. Ware, A history of GPS sounding, *Terr. Atmos. Ocean. Sci.*, *11*, 1–20, 2000.

Zavarotny, V., and A. G. Voronovich, Scattering of GPS signals from the ocean with wind remote sensing application, *IEEE Trans. Geosci. Remote Sens.*, *38*, 951–964, 2000.

A. de la Torre, Departamento de Fisica, FCEyN, Universidad de Buenos Aires, Pab I, Ciudad Universitaria, 1428 Buenos Aires, Argentina. (delatorr@df.uba.ar)

K. Hocke, Communications Research Laboratory, Space Sciences Division, Ministry of Posts and Telecommunications, 4-2-1 Nukui-Kitamachi, Koganei, Tokyo 184-8795, Japan. (hocke@crl.go.jp)

T. Tsuda, Radio Science Center for Space and Atmosphere, Kyoto University, Uji, Kyoto 611-0011, Japan. (tsuda@kurasc.kyoto-u.ac.jp)

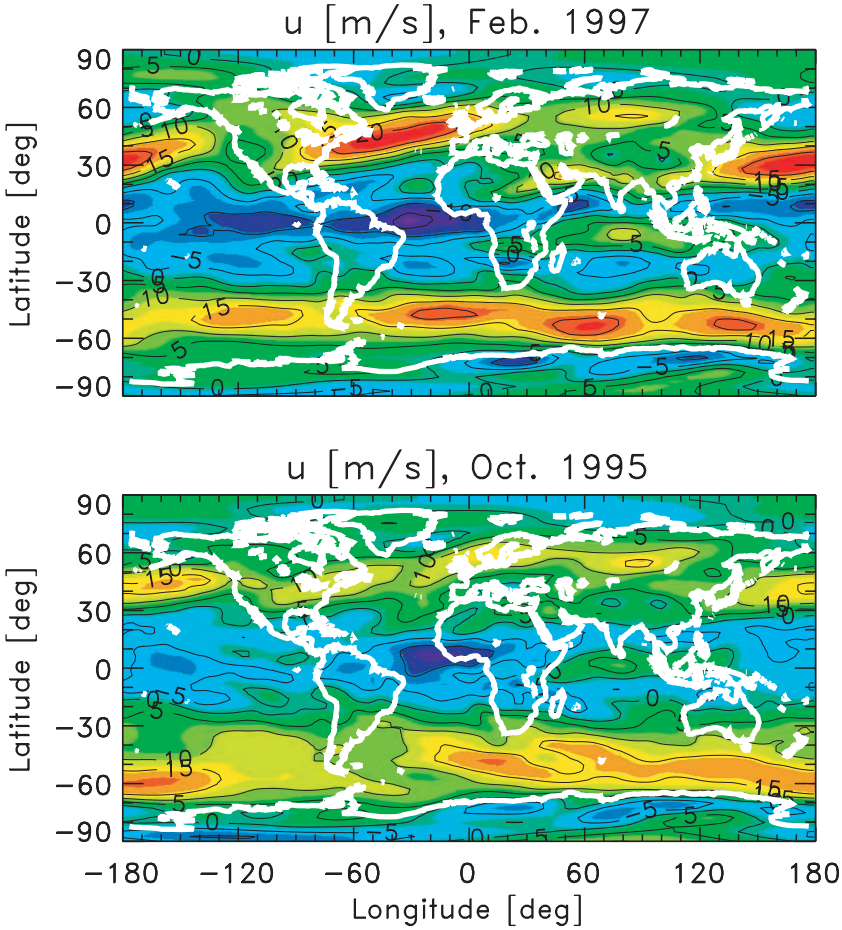

Figure 1. Global map of zonal wind at pressure level 700 mbar in February 1997 (top) and October 1995 (bottom). Red (blue) color denotes eastward (westward) wind direction respectively. Contour labels are in [m/s]. The zonal wind data were calculated and provided by NCEP/NCAR reanalysis and Climate Diagnostics Center (CIRES/NOAA).

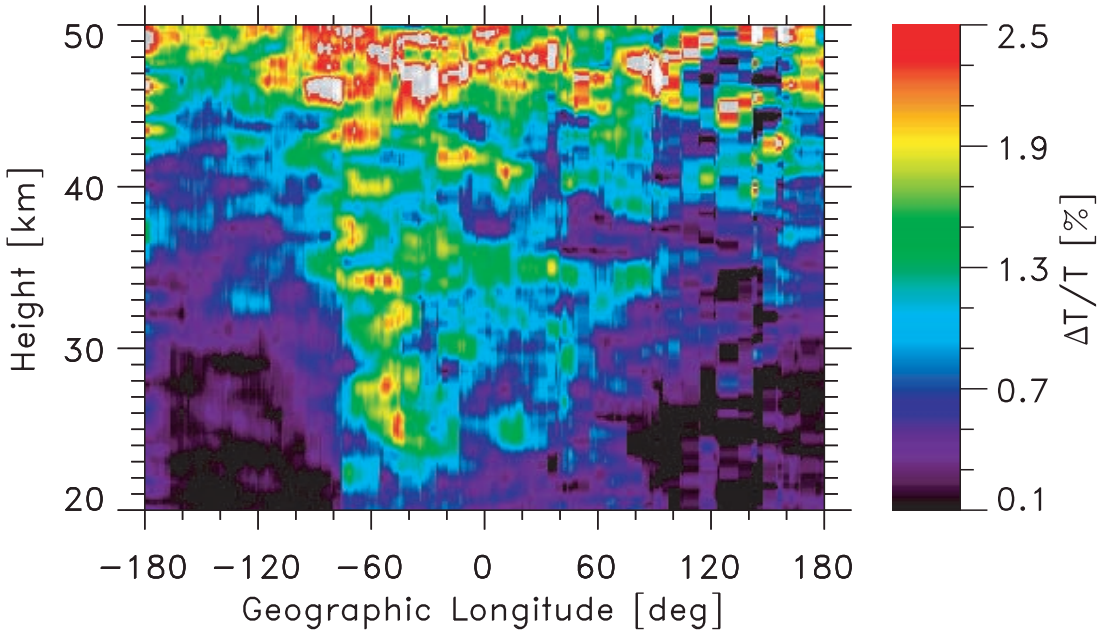

Figure 5. Normalized temperature fluctuations (vertical scales <10 km, $\Delta T/T = |T - \overline{T}|/\overline{T}$) as function of longitude and height for October 1995 at southern midlatitudes (40°–55°S). Vertical wavelength at −70° (70°W) is around 6 km (vertical distances between $T/\overline{T}$ maxima are around 3 km and correspond to the half of the wavelength).

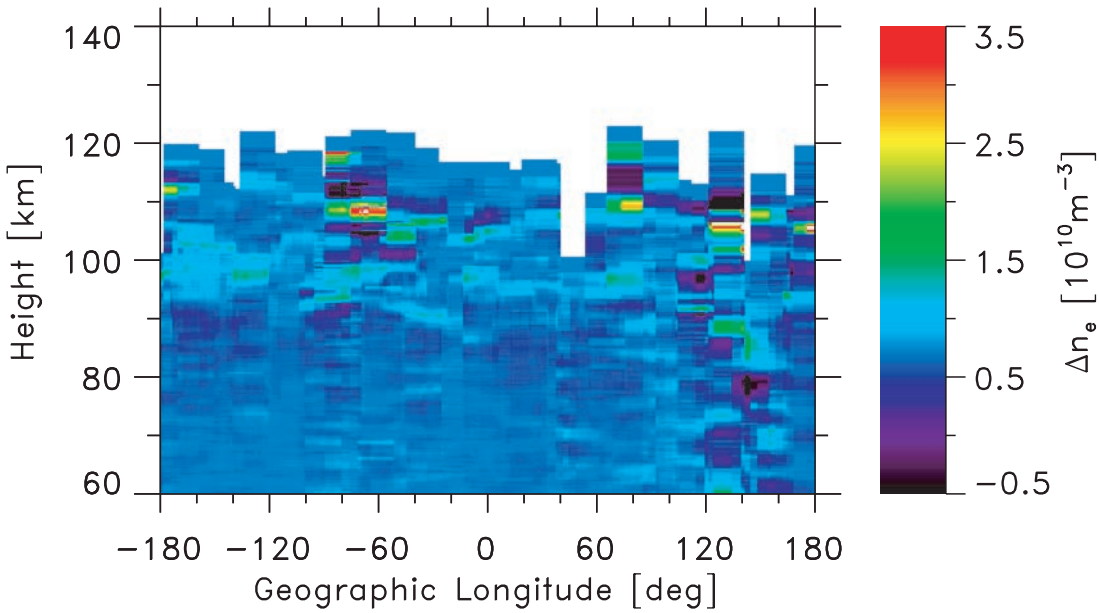

Figure 6. Average plasma density fluctuations (vertical wavelengths less than 7 km) for October 1995 at latitudes 40°–55°S. Around 108 km height and −70° (70°W) a plasma density increase is visible over Andean mountain ridge. Average has been taken with respect to sign of Δn_e.

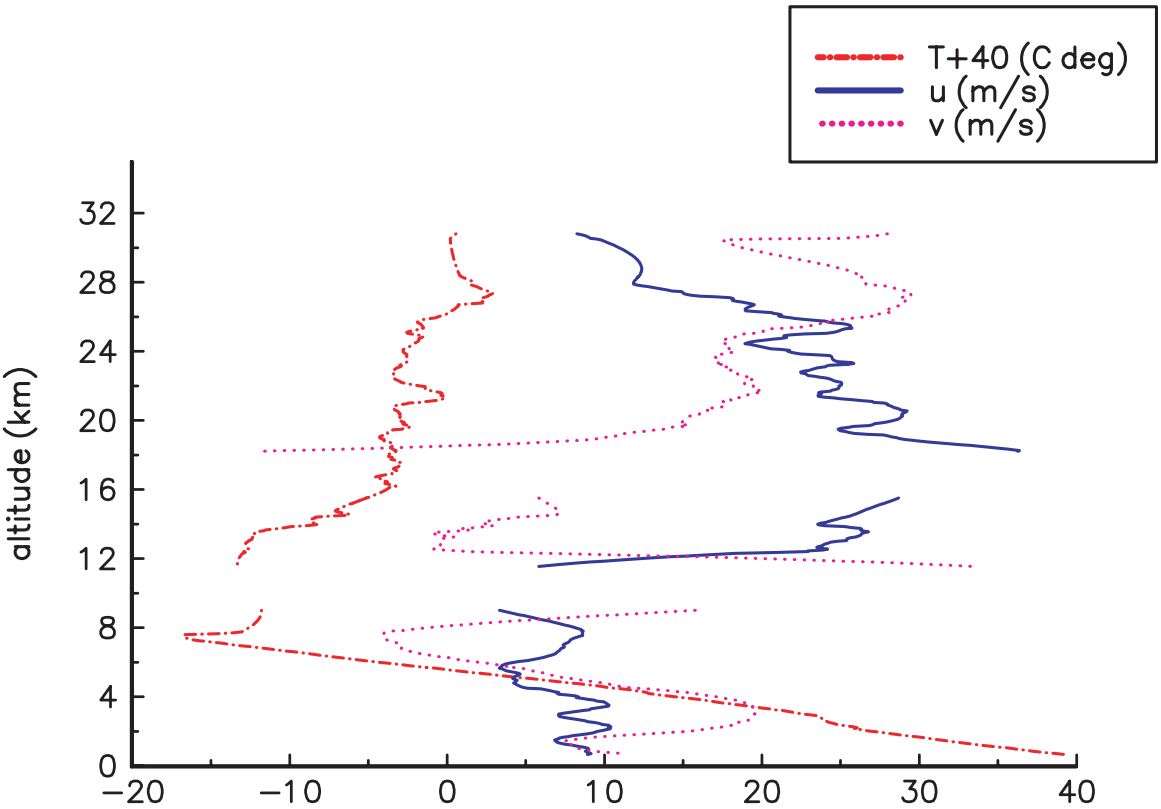

Figure 8. Radiosonde vertical profiles of air temperature T and zonal and meridional wind velocities u and v. Radiosonde launch has been on 24 October 1995 at Ushuaia (54.7°S, 68.1°W).